



Lower head temperature fields for corvis experiments with oxidic melt

Fokkens J.H.⁽¹⁾, Duijvestijn G.⁽²⁾, Braam H.⁽¹⁾

(1) ECN-Nuclear Energy, The Netherlands

(2) Paul Scherrer Institut (PSI), Switzerland

ABSTRACT

The CORVIS (Corium Reactor Vessel Interaction Studies) programme investigated the possible failure modes of a Reactor Pressure Vessel (RPV) lower head induced by direct contact with molten core material following a severe accident. The investigations included experiments and analyses. This paper presents the analysis of lower head thermal behaviour. Topics covered are the heat transfer by convection in the melt, crust formation at the interface between melt and colder structures, and the heat resistance at the interface due to imperfect thermal contact and the development of a gap.

1 INTRODUCTION

During a severe accident in a light water reactor molten core material, or corium, will move downwards and might come in direct contact with the RPV lower head. The project CORVIS was a research programme, conducted by the Paul Scherrer Institute (PSI), with experimental and analytical investigations of possible failure modes of the RPV during a severe accident. To simulate a core meltdown a melt produced with a thermite charge was poured into a test vessel. After melt pouring an electric arc heater was submerged to provide sustained heating. Details of the CORVIS project and current results can be found in [1]. The main objective of the investigations described in this paper is the determination of the heat transfer behaviour of an oxidic melt within steel RPV structures. Important modelling topics in this paper are the heat transfer by convection in the melt, the crust formation of the melt at the interface with colder structures, and a possible increase of the heat resistance as the result of a gap opening at the interface between crust and structure. Ideal would be a coupling between the mechanical and thermal behaviour of the interface between melt and structure, but at this stage only decoupled analyses have been performed. The present paper

concentrates on the thermal behaviour.

A scheme of the test geometry is shown in the figures 1 and 2. The cylindrical test vessel had an internal diameter of 600 mm. In CORVIS experiment 01/11 [2] the test vessel was filled with 420 kg of molten almost pure aluminium oxide. The melt was heated with a double concentric electrode arc heater with a sustained electric power of 200 kW. In earlier studies [1] it was found that the effective heating power can depend on the experimental conditions and is at most 50%.

2 COMPUTATIONAL METHOD

ECN and PSI investigate the thermal behaviour with the respective multi-purpose finite element (FE) codes, MARC and ADINA. The ECN investigation focuses on the phenomenological modelling of the heat transfer by convection in the melt and the crust and pool formation at the melt-structure interface. The PSI study concentrates on the analytical evaluation of the experimental conditions.

The thermal analyses include heat conduction, free convection and radiation, heat input and phase changes. When the debris is liquid, con-

vection can strongly enhance the heat transport. To avoid onerous fluid flow calculations, a solid material conduction-based model is used, as in previous thermal analyses [3, 4]. To simulate heat transfer by convection in a solid element conduction model a modified heat transfer coefficient was introduced. Above the melting temperature of the debris the heat conduction coefficient was increased to a very high value. For the case of an iron melt, this model showed good agreement between measured and calculated temperatures in the bottom plate. As a consequence of the high heat conduction in the melt the temperature distribution in the melt was almost uniform. Due to the different behaviour of an oxidic melt, a more sophisticated treatment is necessary, as described below.

2.1 The conductivity multiplier

For an oxidic melt it is expected that crust formation will take place, which will sharply reduce the heat transfer to the bottom plate. The model previously used, in which the conductivity was increased immediately at the melting point, showed almost uniform temperature distribution in the melt, and no significant crust formation. A gradual increase of the multiplier over a transition temperature range is necessary to simulate crust formation in a solid element model. Therefore a new relation for the modified heat transfer coefficient λ^* is introduced. Using the true conductivity as a base, various temperature dependent multiplier curves are adopted.

$$\lambda^*(T) = \lambda(T) \cdot f_\lambda(T)$$

In order to capture the increased heat transfer above the melting point the following power law is assumed to be an appropriate form for the conductivity multiplier:

$$f_\lambda(T) = \begin{cases} 1 & , T \leq T_m \\ 1 + \frac{49}{(T_1 - T_m)^p} \cdot (T - T_m)^p & , T_m < T \leq T_1 \end{cases}$$

with:

$$\begin{aligned} T_m &= 2050^\circ\text{C} \text{ (melting temperature of Al}_2\text{O}_3\text{)} \\ T_1 &= 2400^\circ\text{C} \end{aligned}$$

For $T > 2400^\circ\text{C}$ λ^* is linearly interpolated between $\lambda^* = 1250$ for $T = 2400^\circ\text{C}$ and $\lambda^* = 10000$

for $T = 3000^\circ\text{C}$.

The parameter p has been varied in the FE-analyses, as summarized in table 1. Figure 3 shows λ^* for $p = 1, 3, \text{ and } 5$.

Table 1 ECN - Perfect Contact at the interface

PC-series	λ^* [W m ⁻¹ K ⁻¹]
PC1	λf_λ $p = 3$
PC2	λf_λ $p = 1$
PC3	λf_λ $p = 5$
PC4	λ
PC5	λ $T < 2050^\circ\text{C}$ 10000 $T > 2050^\circ\text{C}$

2.2 Heat links at the interface

The influence of the heat resistance at the interface between melt and bottom plate is investigated using so called heat link elements at this interface. Heat links are one-dimensional elements with no heat capacity and a heat transfer coefficient which is controlled by a specified conductivity.

Table 2 ECN - temperature independent Heat Link elements at the interface

HL-series	h_{HL} [W m ⁻² K ⁻¹]
HL1	500
HL2	1000
HL3	2500
HL4	5000

Table 3 ECN - temperature dependent Heat Link elements at the interface

HL-series	h_{HL} [W m ⁻² K ⁻¹]	
	low	high
HL12	500	1000
HL13	500	2500
HL23	1000	2500
HL24	1000	5000
HL34	2500	5000

Three separate mechanisms that control the behaviour at the interface between melt and structure are considered:

- 1) Perfect contact;
- 2) Temperature dependent heat resistance due to

imperfect contact;

3) Time dependent heat resistance caused by an opening gap.

To model the heat resistance (case 2) first heat links are introduced with a constant heat transfer coefficient h_{HL} , ranging from 500 to 5000 $Wm^{-2}K^{-1}$, as specified in table 2. Second, a number of analyses are performed with temperature dependent heat links. The heat transfer coefficient is ramped between its values at solidus and liquidus as given in table 3.

2.3 Evaluation of the experiment

CORVIS experiment 01/11 [2] is analysed in detail. In particular the effective heater output and the influence of the interface heat resistance in the presence of a gap are examined. From experimental observations the heater effectivity was expected to be substantially lower than 50%. Heat resistance of a gap of several μm was expected to be between 200 and 500 $Wm^{-2}K^{-1}$ [5]. The assumed conditions are summarized in the tables 4 and 5.

Table 4 *PSI analyses - determination of the effective heater output*

	Effective heater output	
	Perfect Contact	Gap 500 $W m^{-2} K^{-1}$
50%	EPC1	EHL1
35%	EPC2	EHL2
20%	EPC3	EHL3
no power	EPC4	EHL4

Table 5 *PSI analyses - determination of the influence of the gap resistance*

	Gap heat resistance [$W m^{-2} K^{-1}$]
A1	250
A2	500
A3	1000
A4	stepped: 500 / 500,000
A5	variable: 500-200 / 500,000
A6	time dependent: 500,000 / 500-200

In the series EPC and EHL, the influence of effective heater input is investigated by imposing an effectivity factor on the electric power history. The series A uses a value of 20% for the

effectivity. For the cases 'stepped' (A4) and 'variable' (A5) a temperature dependent interface/gap conductivity is adopted. Comparison of the results with experimental data indicate that the interface/gap heat resistance might have been changing with time due, perhaps, to mechanical response of the structure. This analysis does not consider coupling of the mechanical and thermal behaviour. Therefore the gap opening behaviour is fed manually into the thermal analysis. For the case A6, a time dependent interface/gap conductivity is defined, according to the measured deformation. It is assumed that an oxide crust formed instantly upon contact. Observations show that the crust is strong enough to support the weight of the melt. In the first phase of the experiment the bottom plate bent upwards, which enhanced the contact in the central region. After 500 sec. the bottom plate started to sag, which might have induced an opening of the gap. After 1200 sec. the central part of the bottom plate deformed upwards again. Reclosing of the gap, and also perhaps, local remelting of the crust in the central region might have occurred. This behaviour is specified by a time dependent interface/gap conductivity with the following history: 0-500 sec. perfect contact, decreasing to 200 $Wm^{-2}K^{-1}$ at 1500 sec., and increasing to 500 $Wm^{-2}K^{-1}$ after 2000 sec.

3 RESULTS

3.1 Effect of multiplier on crust behaviour

In this section perfect contact on the interface is considered and the effect of different treatments of the conductivity multiplier on crust formation is examined. The results are summarized in figures 4 and 5. The case with no conductivity enhancement (PC4) and with the jump in the conductivity (PC5) are added for comparison. Figure 4 shows the temperature history at two positions at the centre line of the test vessel: position N1 at the interface and position N3 at the outside of the bottom plate. Figure 5 shows the thickness of the crust and the depth of the pool of molten steel as a function of time at the centre of the test vessel. The crust builds up rapidly during the first few minutes before subsequently remelting. It is worth noting that despite the existence of a crust, the bottom plate begins to melt when the crust thickness has been reduced to about 5 mm.

All of the cases calculated show crust formation, and melting of the bottom plate, but the transient behaviour and the crust thickness depends on the form of the multiplier. In particular, use of an immediate jump in conductivity leads to an almost uniform melt temperature, hence only a thin crust which remains at a constant thickness, and earlier initiation of melting. Results clearly indicate the necessity of a power law but the influence of the parameter p in the power law has only a small effect. In the remaining calculations a value $p = 3$ is chosen to achieve a smooth transition.

3.2 Effect of interface heat resistance

The results for different treatment of heat resistance are given in figures 6, 7, and 8. Figure 6 shows that the temperature jump across the interface increases with the heat resistance. In more detail the temperature evolution depends on the form of heat resistance model. The effect on the outside surface is only small as seen from figure 7. Figure 8 shows that increasing the heat resistance decreases the maximum thickness of the crust and leads to earlier melting of the bottom plate. All of the cases with an interface heat resistance exhibit complete remelting of the crust, in contrast to the cases with perfect contact.

3.3 Analytical evaluation experiment

An uncertainty is the effective heat input. In the EHL and EPC series a range of heating effectiveness is considered in an attempt to evaluate the true experimental conditions. Based on the agreement in the later stage of the experiment, where a steady state is developed, we choose an effective heat input of 20 %.

Different treatments of the interface/gap heat resistance are examined in the A-series (table 5). Figures 9, 10, and 11 show the comparison between the thermocouple measurements and the analytical results of the A-series. The position of the thermocouples is shown in figure 1. The results all show an underprediction of the temperature increase during the first 1000 sec. This suggests that the efficiency of the arc heater was initially higher and decreased in the course of the experiment. This can be explained by generation of aerosols and vaporization of carbon due to the very high temperatures in the arc plasma region.

Very good agreement was found in the outer

perimeter of the melt, at TC17. This corresponds with the post test observations [2], and is schematized in figure 2. A stable crust forms in the corners of the melt pool directly upon contact. Comparison of the temperature histories for TC25, TC29 and TC32 show a good agreement in the later phase of the experiment. Results indicate that a interface/gap heat resistance between 250 and 500 $\text{Wm}^{-2}\text{K}^{-1}$ shows best agreement. Increasing the interface/gap conductivity for temperatures above the melting point does not have a large effect on progression of the temperature front.

The temperatures in the central region of the test section exhibit a decrease between 2000 and 3000 sec, after which they rise again. This effect could not be explained in terms of a purely temperature dependent heat resistance. Obviously the interface/gap conductivity can be expected to change due to other factors, which might have modified heat transfer. Closing of the gap may have occurred due to different expansion and deformation of both crust and bottom plate. The time dependent gap conductivity applied in case A6 captures the behaviour satisfactorily. This is interesting also in relation to findings of the TMI-2 [6] accident, where analysis with a conventional approach to modelling also overpredicts the heat up of the RPV structure. It would appear that in this case also the mechanical behaviour of a gap on the interface has influenced the heat up sequence, as was referred to in section 2.3.

4 CONCLUSIONS

Modern FE-codes provide the means for the modelling of the thermal behaviour of and interaction between two non-coherent materials. Analysis has demonstrated how the tools can be applied to interactions between a simulated oxidic core melt pool and colder RPV structures, including phase changes, and dynamic gap behaviour at the interface. Imperfect contact results in a thermal resistance at the interface in the approximate range of 250 to 500 $\text{Wm}^{-2}\text{K}^{-1}$.

Convection within the melt is satisfactorily modelled by a large multiplier on the conductivity. A temperature dependent power law has been used for the transition from the convection dominated heat transfer in the liquid phase, to solid conduction. The form of the transition is shown to control the crust behaviour.

Comparison with experimental results indicates feedback between the mechanical response and the heat transfer at the interface. In order to capture this feedback the calculation method should be extended to include dynamic coupling of the mechanical and thermal behaviour, in particular with respect to the gap. The heat resistance at the interface has a major bearing on whether or not the lower head will fail.

5 ACKNOWLEDGEMENTS

The authors wish to thank Dr. B. Jäckel for his assistance in processing the experimental data, and Dr. J. Birchley in preparation of the paper. The Bundesamt für Bildung und Wissenschaft (BBW) of Switzerland supported this work through contract BBW-No. 95.0060, in conjunction with the Commission of the European Communities through contract No. FIAS-CT95-0002. We thankfully mention the financial assistance to the experimental programme from the Swiss Federal Nuclear Safety Inspectorate (HSK) and the Swiss Federal Office of Energy (BEW). PSI expresses thanks to all 20 task force partners for their contribution to the CORVIS programme and the fruitful cooperation.

The work of ECN Nuclear Energy was supported by the Ministry of Economic Affairs of the Netherlands.

REFERENCES

- [1] S.Brosi, et.al: *CORVIS: Investigation of LWR Lower Head Failure Modes*. Nuc. Eng. & Design., (to be published).
- [2] H.Hirschmann, B.Jäckel, J. Patorski: *CORVIS: Report on Experiment 01/11*. PSI-TM-49-96-04, (published in CORVIS report NO. 7 - editor H. Hirschmann).
- [3] G.Duijvestijn, R.Rösel, S.Brosi: *CORVIS: Investigation of LWR Lower Head Failure Modes - Computational Analysis of Structural Behaviour*. SMiRT-12, Volume U, Paper 07/3, pp. 141-145.
- [4] H.Braam, J.H.Fokkens: *Temperature Analyses for CORVIS Experiments with Oxidic Melt*. ECN-I-96-025, June 1996.
- [5] J.E.Garnier, S.Begej: *Ex-reactor Determination of Thermal Gap and Contact Conductance between Uraniumdioxide:Zircaloy-4 Interfaces*. NUREG/CR-0330, PNL-2692, Pacific Northwest Laboratory, (1979).
- [6] J.Wolf, J.Rempe, (compilers): *TMI-2 Vessel Investigation Project Integration Report*. OECD-NEA-TMI-2, Vessel Investigation Project TMI V (93) EG10, (1993).

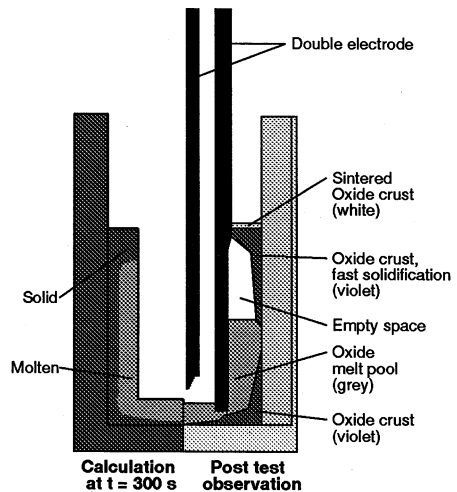
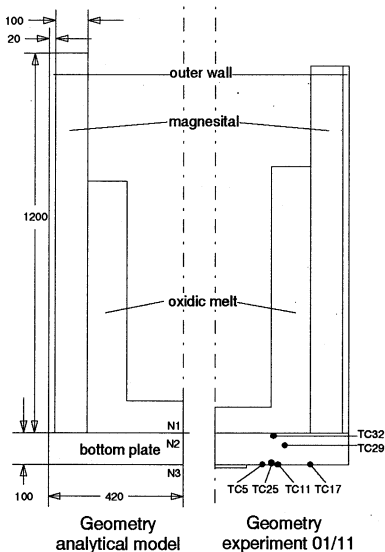


Figure 1 Geometry of the used analytical model and of experiment 01/11

Figure 2 Comparison of analytical and experimental results

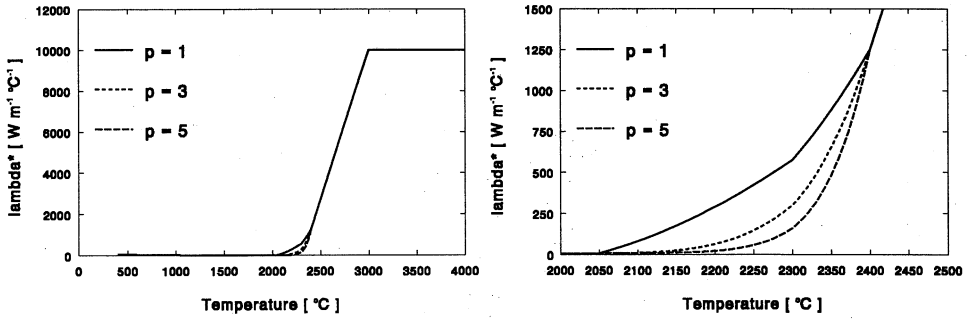


Figure 3 The modified thermal conductivity of Al_2O_3 as a function of temperature
Temperature range $0 < T < 4000$ and $2000 < T < 2500$

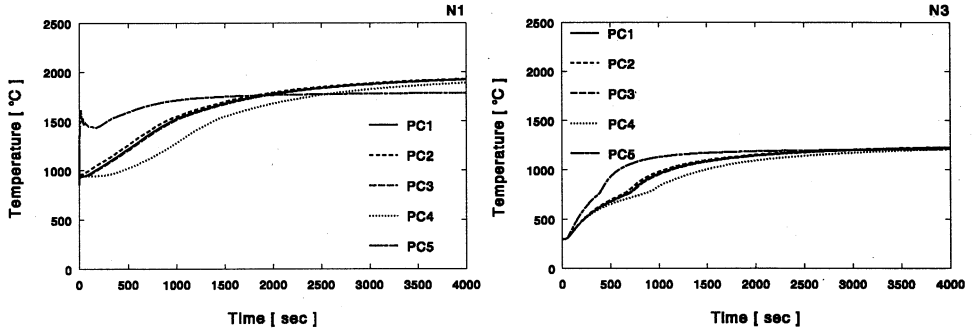


Figure 4 Analyses with perfect contact at the interface (PC-series)
Temperature history at position N1 and N3 as depicted in figure 1

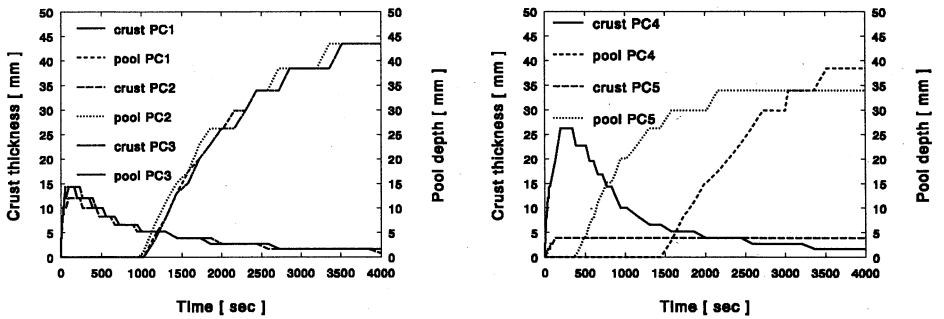


Figure 5 Analyses with perfect contact at the interface (PC-series)
Thickness of the crust and depth of the pool of molten steel at the centre line ($r = 0$ mm)
as a function of time

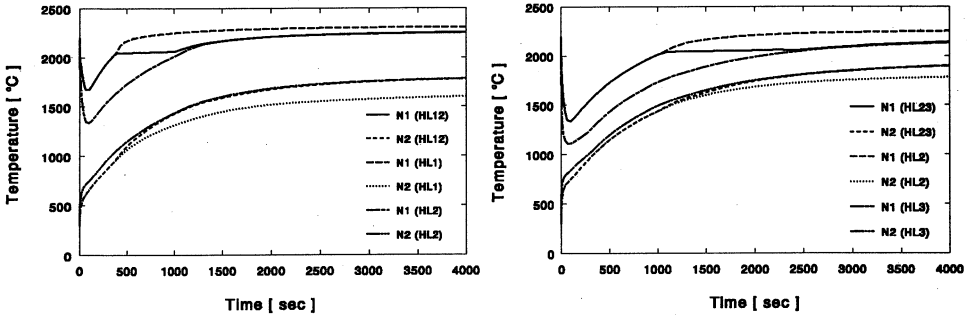


Figure 6 Analyses with heat links at the interface (HL-series)
 Temperature history at position N1 and N2 as depicted in figure 1 for case HL1, case HL2, case HL3, case HL12, and case HL23

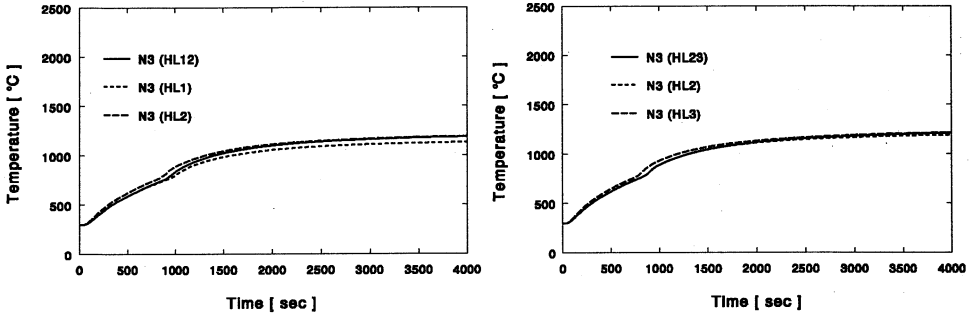


Figure 7 Analyses with heat links at the interface (HL-series)
 Temperature history at position N3 as depicted in figure 1 for case HL1, case HL2, case HL3, case HL12, and case HL23

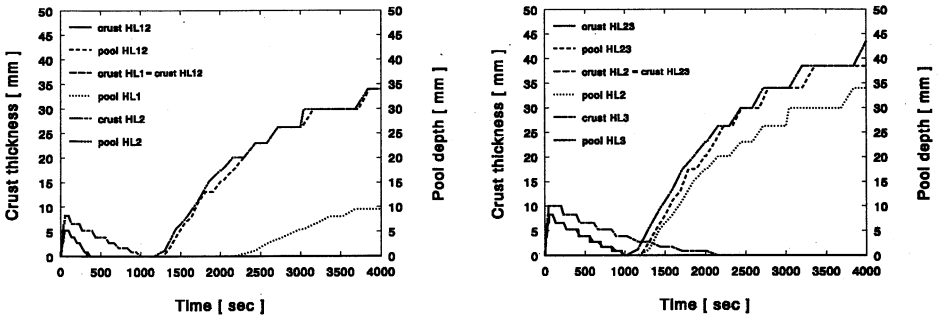


Figure 8 Analyses with heat links at the interface (HL-series)
 Thickness of the crust and depth of the pool of molten steel at the centre line ($r = 0$ mm) as a function of time for case HL1, case HL2, case HL3, case HL12, and case HL23

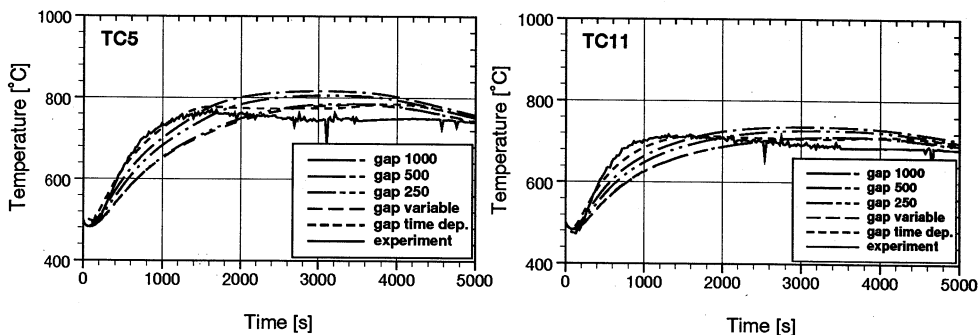


Figure 9 Additional analyses for the evaluation of the experiment (A-series)
Comparison of the calculated and measured temperatures at the locations of thermocouple 5 and 11

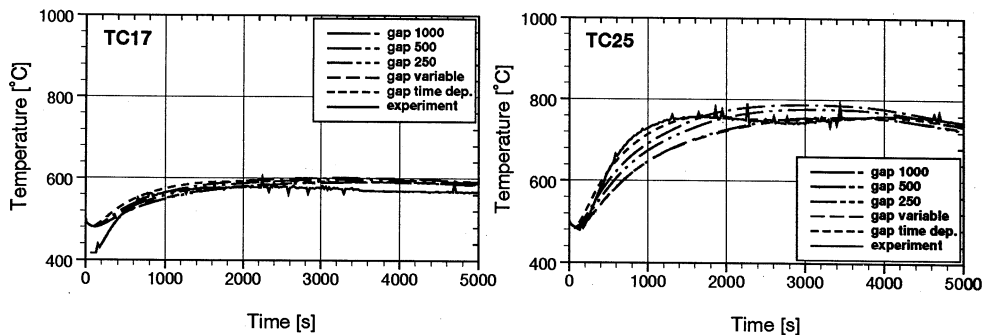


Figure 10 Additional analyses for the evaluation of the experiment (A-series)
Comparison of the calculated and measured temperatures at the locations of thermocouple 17 and 25.

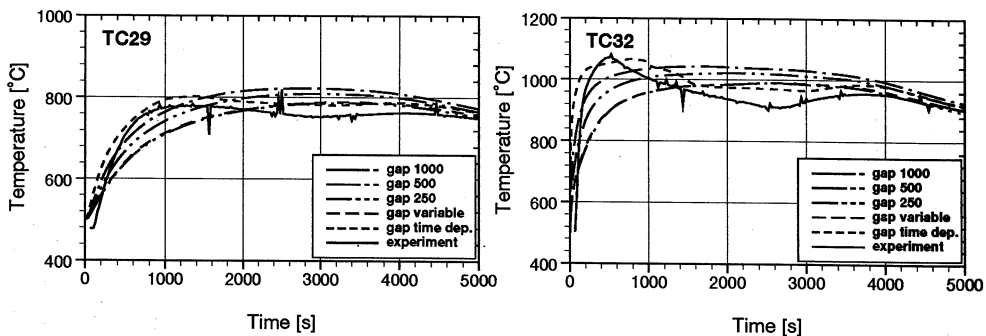


Figure 11 Additional analyses for the evaluation of the experiment (A-series)
Comparison of the calculated and measured temperatures at the locations of thermocouple 29 and 32